Journal of Alloys and Compounds 509 (2011) 9724–9732

Contents lists available at ScienceDirect

Journal of Alloys and Compounds

journal homepage: www.elsevier.com/locate/jallcom

The magnetic structures of RMgSn compounds (R = Ce, Pr, Nd, Tb)

C. Ritter[a,*], A. Provino[b,c,d], P. Manfrinetti[b,c,d], K.A. Gschneidner Jr.[b]

[a] Institut Laue-Langevin, Boite Postale 156, F-38042 Grenoble, France
[b] Ames Laboratory-US DOE and Department of Materials Science and Engineering, Iowa State University, Ames, IA 50011-3020, USA
[c] Dipartimento di Chimica e Chimica Industriale, Università di Genova, Via Dodecaneso 31, 16146 Genova, Italy
[d] CNR-SPIN, Corso Perrone 24, 16152 Genova, Italy

ARTICLE INFO

Article history:
Received 13 July 2011
Received in revised form 26 July 2011
Accepted 29 July 2011
Available online 4 August 2011

Keywords:
Rare-earth magnesium stannides
Crystal structure
Neutron diffraction
Magnetic ordering
Magnetic structure

ABSTRACT

The synthesis of the new compounds RMgSn (R = La–Nd, Sm, Gd–Tm, Lu and Y) has been recently reported. The compounds formed by La and Ce crystallise in the TiNiSi structure type (*oP*12, *Pnma*), while from Nd they adopt the CeScSi-type (*tI*12, *I*4/*mmm*); PrMgSn is dimorphic: its high-temperature form (HT) is TiNiSi-type while the low-temperature one (LT) is CeScSi-type.

In this paper we now report the results of a neutron diffraction investigation which has been performed in order to refine the crystal as well as the magnetic structures for the RMgSn compounds with R = Ce, Pr, Nd and Tb. All these compounds see at low temperature the establishment of long range magnetic ordering with a predominantly antiferromagnetic interaction; only PrMgSn-HT orders ferromagnetically. These results agree with those from magnetic measurements recently reported.

The magnetic structure of CeMgSn is of the amplitude-modulated type, the value of the magnetic propagation vector refined at 2 K is τ = [0, 0.1886(4), 0.3384(8)]. The PrMgSn-HT phase below T = 52 K adopts first a purely ferromagnetic structure, then at about T = 15 K a second magnetic coupling leads to a spin-canted magnetic structure. Both PrMgSn-LT and NdMgSn have the same antiferromagnetic commensurate magnetic structure. The TbMgSn compound below T_N = 35 K orders antiferromagnetically with an equal moment cycloidal structure; however a second magnetic transition at a temperature corresponding to T_{N2} = 65 K is likely also present.

1. Introduction

The formation, crystal structures and melting behaviour of the two new families of rare earth intermetallic RMgSn [1,2] and RMgPb [3] phases have been reported recently. Previously to these reports no ternary R-Mg-X (X = Sn and Pb) compounds have ever been reported [4–6], but R = Eu and Yb. All the rare earth elements form the 1:1:1 equiatomic compounds: the RMgSn family extends from La to Lu including Y but not Sc, while in the RMgPb series also both YMgPb and ScMgPb compounds form. Differential Thermal Analysis showed that all the RMgX compounds (X = Sn and Pb) form congruently, the melting temperature lowering on going from the light to the heavy R [1]. The RMgSn compounds have been found to crystallize in two different structure types: the RMgSn phases with the lighter R (R = La, Ce, Pr) adopt the orthorhombic TiNiSi structure type (Fig. 1a, an ordered derivative of the Co_2Si-type, *oP*12, *Pnma*), while the ones formed by the heavier R (R = Nd, Sm, Gd, Tb, Dy, Ho, Er, Tm and Lu, plus Y) form in the tetragonal CeScSi-type structure (Fig. 1b, an ordered derivative of the La_2Sb-type, *tI*12, *I*4/*mmm*) [1].

For PrMgSn, the synthesis conditions and a lower annealing temperature (700 °C) adopted by Lemoine et al. [2] allowed the formation of a low temperature phase (PrMgSn-LT), showing CeScSi-type structure. In the case of RMgPb series, all the compounds are isomorphic adopting the CeScSi-type crystal structure. Crystallographic considerations suggested a room-temperature trivalent state for Ce and Sm and a divalent state for Yb, in both the stannides and plumbides.

Measurements of the heat capacity, magnetization and electrical resistivity on most members of these two series of compounds have been carried out. Some preliminary results were already reported [7], while a more enlarged report about the physical properties of both the RMgSn and RMgPb families is going to be published [8]. We found that the compounds with a magnetic R generally order antiferromagnetically with Néel temperatures ranging in between 8 and 80 K, the higher ordering temperature pertaining to SmMgSn with a T_N of about 81 K. The magnetic ordering temperatures of corresponding members in the two families of compounds are comparable. About what is concerning the compounds object of the present work, CeMgSn has been found to order antiferromagnetically with a T_N of about 13 K, with no evidence of Kondo effect (as inferred from the variation of its resistivity with temperature); PrMgSn-HT orders

* Corresponding author.
E-mail address: ritter@ill.fr (C. Ritter).

0925-8388/$ – see front matter © 2011 Elsevier B.V. All rights reserved.
doi:10.1016/j.jallcom.2011.07.100

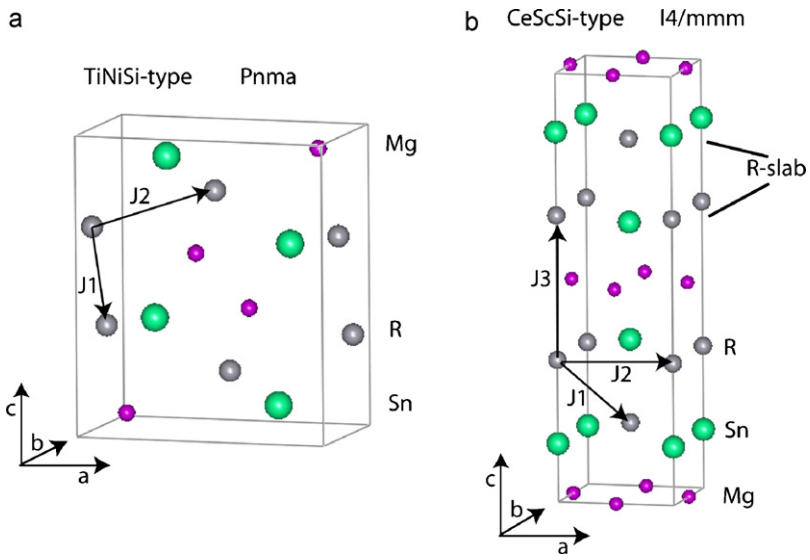

Fig. 1. (a) TiNiSi-type structure adopted by CeMgSn and PrMgSn-HT. (b) CeScSi-type structure adopted by PrMgSn-LT, NdMgSn and TbMgSn. The shortest R–R distances are indicated by arrows.

ferromagnetically with $T_C = 52$ K, NdMgSn and TbMgSn order antiferromagnetically with Néel temperatures of 31 and 34 K, respectively.

Meanwhile our work was in progress, the magnetic properties of the RMgSn compounds were reported in literature by Lemoine et al. [2]; in this latter, antiferromagnetic ordering at $T_N = 20$ K has been reported for PrMgSn-LT. Our results are in good agreement with those of Ref. [2], in what is concerning both the type of magnetic ordering as well the transition temperatures.

Now, in this article, we present the results of a neutron diffraction work performed on the CeMgSn, PrMgSn-HT, PrMgSn-LT, NdMgSn and TbMgSn phases.

2. Experimental details

The samples were prepared into Ta crucibles by induction melting. Weighed amounts of the metals [large pieces of the rare earth, cut from bulk and handled in glove-box (99.9+ wt.% purity, Ames Laboratory), magnesium chunk (99.99 wt.% purity) and pieces of tin (99.999 wt.% purity)], for a total mass of 8–10 g, were placed inside outgassed Ta crucibles which were sealed by arc welding under an inert Ar atmosphere. The alloys were melted by slowly heating up to 1250 °C (±20 °C) (i.e.: about 50 °C above the *liquidus* temperatures of the alloys [1]), then slowly cooled down to room temperature. The crucibles were closed into quartz ampoules under vacuum to be annealed in a resistance furnace. CeMgSn, NdMgSn and TbMgSn samples were heat treated at 900 °C for 7 days, then air cooled; PrMgSn-HT (HT = high temperature), after the same treatment as above, was further treated at 1000 °C for 1 day then ice-water quenched, while PrMgSn-LT (LT = low temperature) was annealed at 650 °C for 7 days and slowly cooled. As already observed in our previous work [1], no contamination by Ta was detected. Phase analysis was performed by X-ray powder diffraction, using a X'Pert diffractometer (Cu Kα_1 radiation); no impurity phases were found in all the prepared samples, if not at a trace level.

The neutron diffraction data were taken on the high resolution powder diffractometer D2B and on the high intensity powder diffractometer D1B, both situated at the *Institut Laue Langevin* at Grenoble, France. D1B has been recently equipped with a new multidetector spanning 120° in 2θ with detector cells every 0.1°. The thermal dependence of the neutron spectra (thermodiffractogram) was determined on D1B with $\lambda = 2.52$ Å for R = Tb, Nd, Pr (HT) and Pr (LT), recording spectra of 5 min every 3 K. Additional data with higher statistics (10 min for R = Tb and Nd and 15 min for the two Pr compounds) were taken at 2 K and above the specific magnetic transition temperature. For CeMgSn spectra with long counting times of about 3 h were used at $T = 2$ K and 20 K. A thermodiffractogram was taken on this compound counting for 15 min every degree. The presence of a 0.6% $\lambda/2$ wavelength contamination was taken into account in the refinements of the D1B data. The high resolution data were recorded on D2B at room temperature using $\lambda = 1.594$ Å between $0° < 2\theta < 160°$ using a step-width of 0.05°. All neutron data were analysed using the Rietveld refinement program FULLPROF [9]; sketches of the crystallographic and magnetic structures were drawn with the program FullProf Studio [10], this latter incorporated in Ref. [9].

3. Results and discussion

3.1. High resolution neutron diffraction

The high resolution data recorded at room temperature were refined in order to determine lattice constants and atomic coordinates and, most importantly, in order to check for the existence of any impurity phases. Refinements proceeded smoothly using the known structure types of TiNiSi (*Pnma*) for R = Ce and Pr (HT) and CeScSi (*I4/mmm*) for R = Pr (LT), Nd and Tb; Table 1 contains the results of these refinements. Fig. 2 displays, by way of example, plots of the refinements of PrMgSn (HT) and NdMgSn.

There were no signs of any significant amounts of impurity phases in any of these five samples. Special attention was given to the analysis of the refinement of PrMgSn (HT) phase, as it is known that the sample could be easily contaminated by the presence of the low-temperature modification PrMgSn (LT). Any attempts to include PrMgSn (LT) as a possible second phase in the refinement of the PrMgSn (HT) data failed and we can exclude its presence above the 2% level.

Table 1
Results of the Rietveld refinement against neutron diffraction data at 300 K for the RMgSn compounds with TiNiSi or CeScSi structure type.

TiNiSi type	Ce	Pr (HT)
x_R	0.0197(3)	0.0202(4)
z_R	0.6819(3)	0.6815(3)
x_{Mg}	0.1546(3)	0.1548(3)
z_{Mg}	0.0683(3)	0.0668(3)
x_{Sn}	0.27185(2)	0.2700(3)
z_{Sn}	0.3882(2)	0.3873(2)
a (Å)	7.7271(2)	7.6801(3)
b (Å)	4.6480(1)	4.6219(2)
c (Å)	9.0818(2)	9.0631(3)
d_{J1}	4.067(10)	4.036(4)
d_{J2}	3.999(5)	4.032(3)
R_{Bragg}	8.7%	6.5%

CeScSi type	Pr (LT)	Nd	Tb
x_R	0.33356(11)	0.33350(5)	0.33231(5)
x_{Sn}	0.13250(9)	0.13290(7)	0.13548(5)
a (Å)	4.49136(7)	4.47190(4)	4.38367(3)
c (Å)	16.2216(3)	16.1445(2)	15.8794(2)
R_{Bragg}	7.5%	3.4%	2.7%

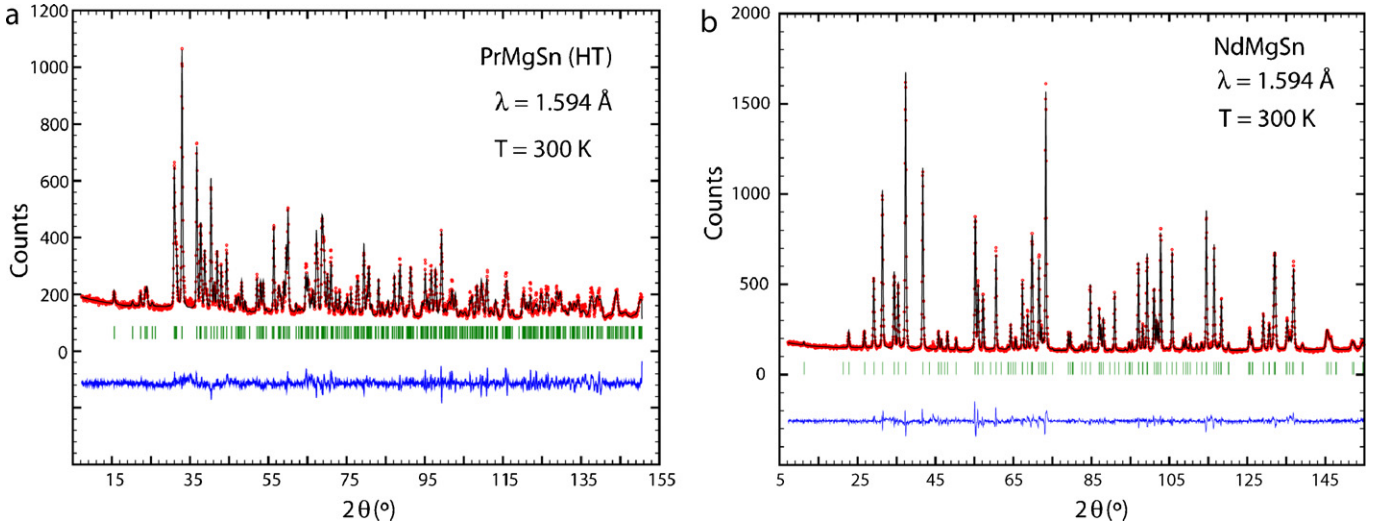

Fig. 2. Observed (dots, red), calculated (line, black) and difference pattern of (a) PrMgSn (HT) and (b) NdMgSn and at 300 K (refined in the *Pnma* and *I*4/*mmm* space groups, respectively). The tick marks indicate the calculated position of the nuclear Bragg peaks. (For interpretation of the references to colour in this figure legend, the reader is referred to the web version of the article.)

3.2. High intensity neutron diffraction

3.2.1. NdMgSn

Fig. 3 displays the thermodiffractogram of NdMgSn which, on lowering the temperature, reveals the appearance of new reflections indicating the antiferromagnetic nature of the magnetic ordering in this compound. The nuclear reflections do not show any change excluding any form of ferro- or ferrimagnetism. Fitting the intensity of the magnetic Bragg peaks as function of temperature the magnetic transition temperature is determined to $T_N \approx 31$ K. This data compare pretty well with the transition temperature of 31 K, as found by Lemoine et al. [2], and the value of 30.5 K we report in Ref. [8].

Fig. 4 shows the magnetic Bragg peaks in form of a difference spectrum created using the data taken at 2 K and 38 K. From the position of the magnetic Bragg peaks the magnetic propagation vector was determined using the program K-Search which is part of the FULLPROF suite of programs to $\tau = [1\,0\,0]$. Due to the *I*-centering present in the structure the vectors $\tau = [0\,1\,0]$ and $[0\,0\,1]$ are equivalent. Magnetic symmetry analysis using the program BASIREPS which is part of the FULLPROF suite of programs [9,11], was employed to determine the allowed irreducible representations (IR) and their basis-vectors (BV), see Table 2 for the Wyckoff position *4e* of Nd in *I*4/*mmm*.

Out of the 4 allowed IR's, two are of purely ferromagnetic character and can be excluded. The other two IR's contained BV's describing a simple antiferromagnetic coupling between the symmetry related rare earth sites. The BV needed to refine the magnetic intensities correctly is directly connected to the choice of the magnetic propagation vector ($\tau = [1\,0\,0]$, $[0\,1\,0]$ and $[0\,0\,1]$ being equivalent). With $\tau = [1\,0\,0]$ the magnetic structure is described using BV1 of IR3, the magnetic moment value at 2 K amounts to $\mu_{Nd} = 2.94(2)\,\mu_B$, corresponding nearly to the expected value for the Nd^{3+} ion ($3.28\,\mu_B$).

Table 2
Basis-vectors (BV) of the four allowed irreducible representations (IR) for $\tau = [1\,0\,0]$ and for Wyckoff position *4e* of space group *I*4/*mmm*.

	BV1	BV2		BV1	BV2
IR1			IR2		
x, *y*, *z*	0 0 1			0 0 1	
−*x*, *y*, −*z*	0 0 −1			0 0 1	
IR3			IR4		
x, *y*, *z*	1 0 0	0 −1 0		0 1 0	1 0 0
−*x*, *y*, −*z*	−1 0 0	0 1 0		0 1 0	1 0 0

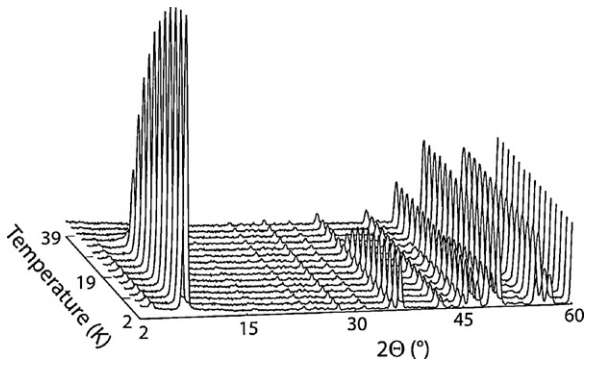

Fig. 3. Thermal dependence of the neutron diffraction pattern (thermodiffractogram) of NdMgSn between 2 K and 39 K.

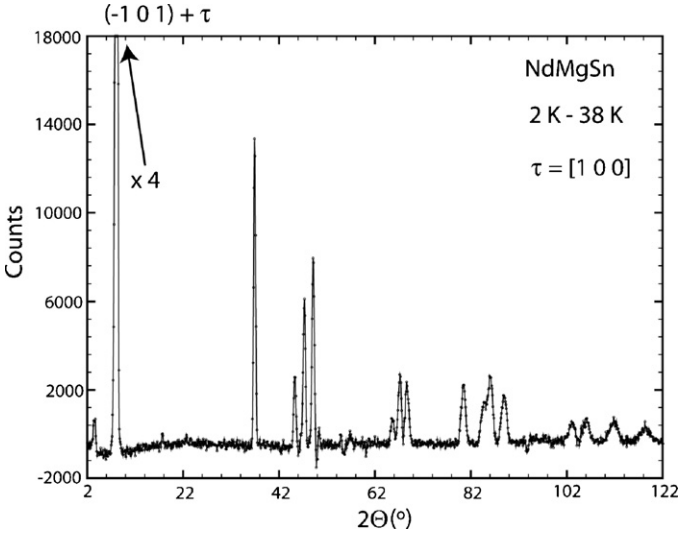

Fig. 4. Difference spectrum 2–38 K showing the purely magnetic scattering of NdMgSn.

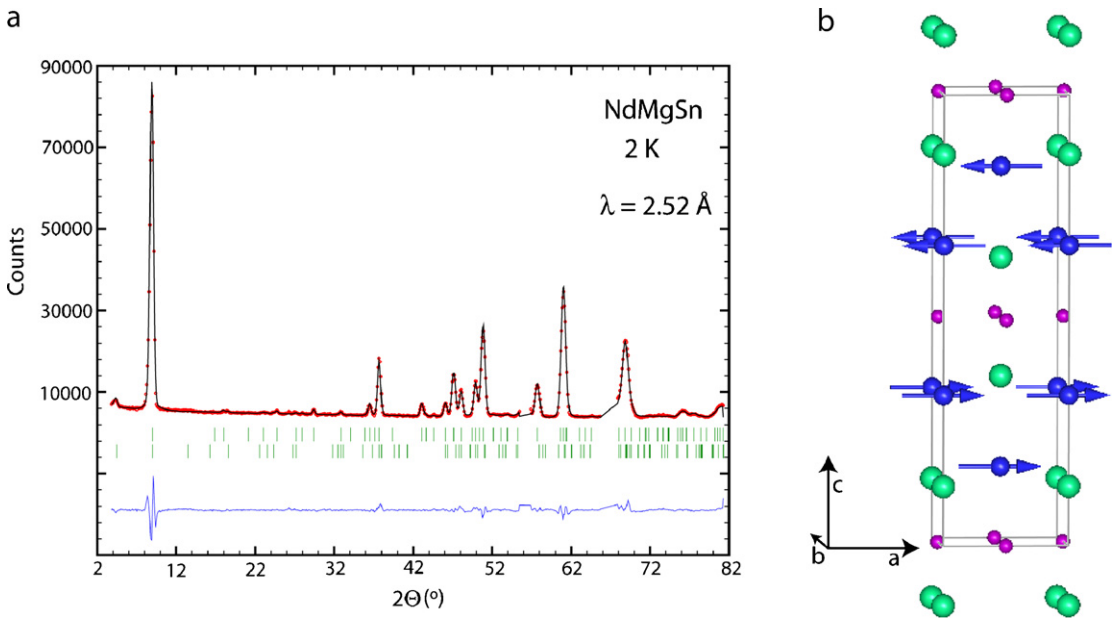

Fig. 5. (a) Observed (dots, red), calculated (line, black) and difference pattern of NdMgSn at 2 K. The tick marks indicate the calculated position of the nuclear Bragg peaks (upper row) and of the magnetic peaks (lower row). (b) Magnetic structure of NdMgSn, pink (green) balls represent the Mg (Sn) atoms. (For interpretation of the references to colour in this figure legend, the reader is referred to the web version of the article.)

Fig. 5a shows the refined spectrum at 2 K, Fig. 5b the magnetic structure which sees an antiferromagnetic coupling in *c*-direction of ferromagnetically aligned layers within the tetragonal basis plane. The direction of the magnetic moments within the *a*–*b* plane cannot be determined from powder data.

3.2.2. PrMgSn (LT)

The thermodiffractogram recorded for the low temperature phase of PrMgSn looks very similar to the one of the Nd compound and is therefore not shown here. The same magnetic peaks appear on lowering the temperature, the fit of the temperature dependence of the magnetic peak intensity gives $T_N = 24$ K, slightly higher if compared with 20 K given for this phase in Ref. [2]. Fig. 6a shows again a difference spectrum (2–73 K) which, when compared to Fig. 4, clearly indicates the strong similarity to the magnetic Bragg peaks found for NdMgSn. Using the same magnetic model the refinement of the 2 K data (Fig. 6b) proceeded smoothly and gave a magnetic moment of $\mu_{Pr} = 2.42(2)\,\mu_B$; value slightly smaller than that expected for the Pr^{3+} ion (3.2 μ_B).

3.2.3. TbMgSn

TbMgSn is the third compound of our series which adopts the CeScSi-type structure. Its thermodiffractogram (Fig. 7) is only at the first glance similar to the ones of R = Nd and Pr (LT). A more detailed inspection reveals that some of the magnetic peaks change slightly their position as function of temperature, this indicates the existence of a temperature-dependent incommensurate magnetic propagation vector. The magnetic transition temperature was again determined from the fit of the magnetic Bragg peak intensities as function of temperature. While most of the magnetic Bragg peaks disappear at $T_N = 35$ K, well corresponding to the value of T_N of 34 K given in Ref. [2], the very strong low angle reflection is still visible

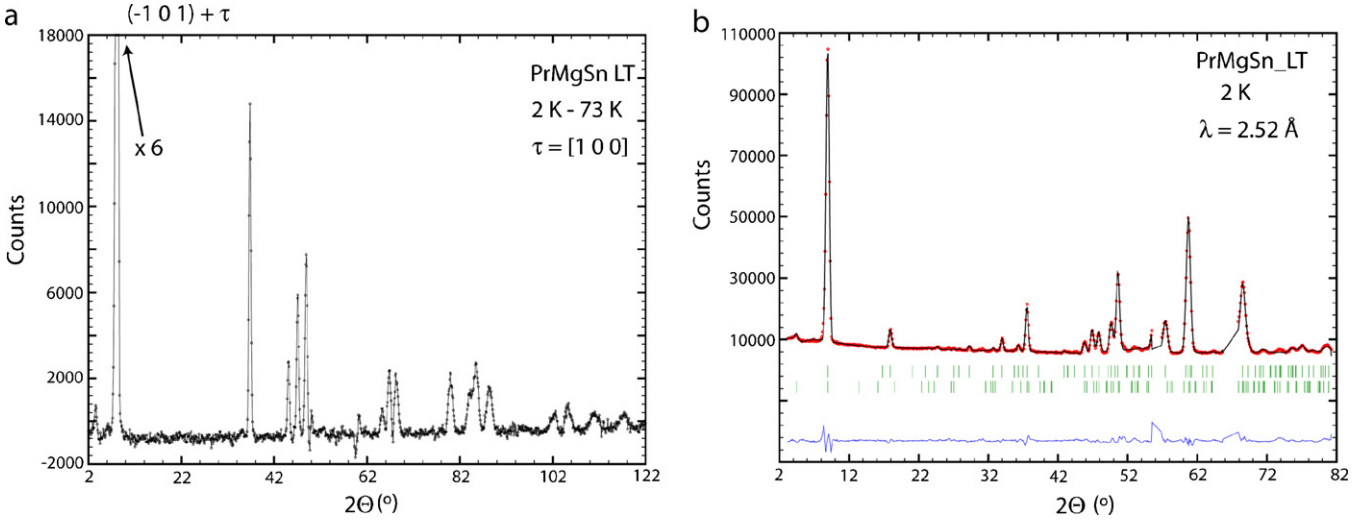

Fig. 6. (a) Difference spectrum 2–73 K showing the purely magnetic scattering of PrMgSn (LT). (b) Observed (dots, red), calculated (line, black) and difference pattern of PrMgSn (LT) at 2 K. The tick marks indicate the calculated position of the nuclear Bragg peaks (upper row) and of the magnetic peaks (lower row). (For interpretation of the references to colour in this figure legend, the reader is referred to the web version of the article.)

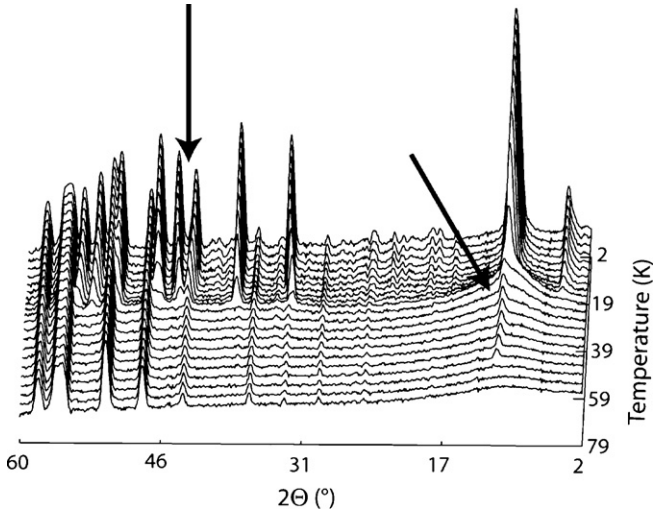

Fig. 7. Thermal dependence of the neutron diffraction pattern of TbMgSn between 2 K and 79 K. The 2θ and the temperature axes are turned with respect to Fig. 2, the intensity is plotted in a logarithmic scale due to the dominance of the low angle peak. Arrows indicate magnetic reflections shifting in 2θ as function of temperature and the persistence of a magnetic peak at $T > T_N$.

on top of a broad bump created by strong short range magnetic ordering up to about 65 K. Fig. 8a displays the difference spectrum (2–75 K) which shows the multitude of magnetic reflections and the dominating intensity of the low angle peak.

From the position of the magnetic peaks the magnetic propagation vector was determined using K-search to $\tau \approx [0.84\,0\,0]$ with $\tau = [0\,0.84\,0]$ being equivalent in the tetragonal system. Magnetic symmetry analysis gives 4 possible IRs which are listed with their basis-vectors in Table 3.

Any attempt to refine the neutron data at 2 K using just one of these IRs failed, but a combination of BV1 of IR1 and BV1 of IR3 gives a perfect fit of the magnetic scattering. As the coefficients for these basis-vectors refined within errors to the same value, they were in the final refinement constrained to be equal without any loss in the goodness of the fit. Fig. 8b displays the fit of the data at 2 K.

Refining incommensurate magnetic structures using neutron powder data, it is not possible to differentiate between amplitude modulated (sine wave) and equal-moment (helix-type) structures. Physical arguments can be used to favour one or the other model. In the case of TbMgSn the value of the magnetic moment refines to $11.9(2)\,\mu_B$ using the amplitude modulated model and to $\mu_{Tb} = 8.4(1)\,\mu_B$ for the equal-moment model. As the expected moment for a Tb^{3+} ion is $9\,\mu_B$, we can reasonable well exclude the sine wave model. Fig. 9 displays the magnetic structure assuming the equal-moment model. It consists of a cycloidal spiral [12] where the spins are confined to the tetragonal a–b plane. Going from one unit cell to the neighbouring in direction of the propagation vector, the spins turn by $360^\circ \times 0.84 \approx 302^\circ$. As in the case of the R = Nd and Pr (LT) compounds, layers of magnetic spins within the a–b plane are antiferromagnetically oriented in the c-direction with respect to the $z = 0.5$ level.

Table 3
Basis-vectors (BV) of the four allowed irreducible representations (IR) for $\tau = [0.84\,0\,0]$ and for Wyckoff position *4e* of space group *I*4/*mmm*.

	BV1	BV2		BV1	BV2
IR1			IR2		
x, y, z	0 1 0			1 0 0	0 0 1
$-x, y, -z$	0 −1 0			1 0 0	0 0 −1
IR3			IR4		
x, y, z	1 0 0	0 0 1		0 1 0	
$-x, y, -z$	−1 0 0	0 0 1		0 1 0	

The temperature dependent data for $2\,K \leq T \leq 33\,K$ were used to refine the temperature dependence of the magnetic moment and of the magnetic propagation vector; for data with $T > 33$ K the value of the magnetic propagation vector was determined from the position of the sharp magnetic (1 0 1) – τ Bragg peak (Fig. 8a). Fig. 10 shows the smooth variation of the value of the magnetic propagation vector, which decreases from $\tau = [0.84\,0\,0]$ at $T = 2$ K down to $\tau = [0.80\,0\,0]$ at $T = 37$ K in parallel to the decrease of the magnetic moment value. Above T_N it stays practically constant up to about $T = 52$ K before a further decrease leads to $\tau = [0.78\,0\,0]$ at $T = 64$ K which represents the highest temperature where the peak is still discernable above the bump linked to short range magnetic ordering. Although only defined by a single magnetic peak we think that it is reasonable to speak of a second magnetic transition temperature in TbMgSn, corresponding to $T_{N2} = 65$ K.

3.2.4. PrMgSn (HT)

The thermodiffractogram of PrMgSn (HT) (not shown here) shows the increase of some nuclear Bragg peaks below about 50 K. Furthermore one can see a magnetic reflection at $2\theta = 15^\circ$ appearing

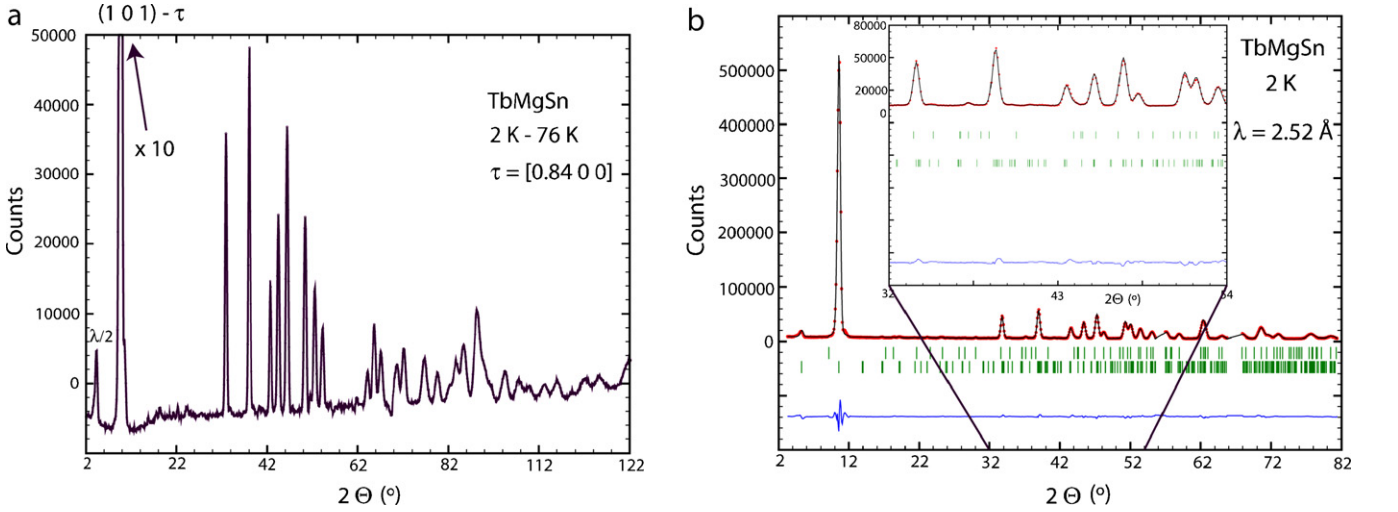

Fig. 8. (a) Difference spectrum 2–76 K showing the purely magnetic scattering of TbMgSn. (b) Observed (dots, red), calculated (line, black) and difference pattern of TbMgSn at 2 K. The tick marks indicate the calculated position of the nuclear Bragg peaks (upper row) and of the magnetic peaks (lower row).

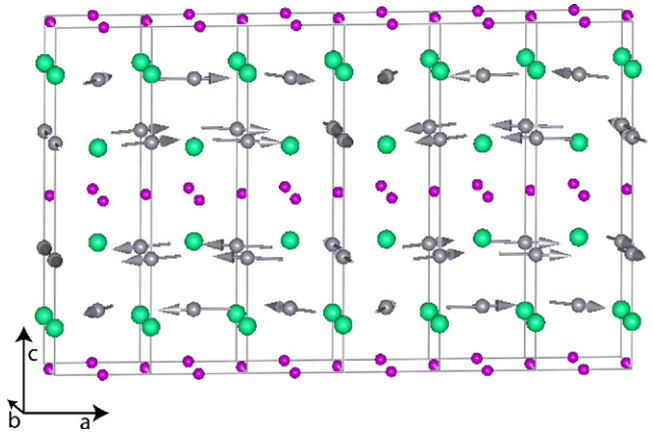

Fig. 9. Magnetic structure of TbMgSn. (For interpretation of the references to colour in this figure legend, the reader is referred to the web version of the article.)

below about 15 K. While the increase of the nuclear peaks indicates that the magnetic coupling is mainly of ferromagnetic nature, the new magnetic peak points to the presence of as well antiferromagnetic interactions.

Fig. 11 displays the difference spectrum (2–58 K) where this peak has been indexed as the (0 0 1) peak, forbidden in the *Pnma* space group. From the position of the magnetic peaks the magnetic propagation vector was determined to $\tau = [0\,0\,0]$. Fitting the temperature dependence of some magnetic Bragg peak intensities the magnetic transition temperature was determined to be $T_C = 52$ K, well confirming the value given in either the Refs. [2,8]. Magnetic symmetry analysis for $\tau = [0\,0\,0]$ gives for the Wyckoff *4c* position of Pr eight IRs, three of which contain ferromagnetic basis-vectors. Refining the 2 K data against the different proposed models only a mixture of 2 IRs was able to account for the measured magnetic Bragg peak intensities. While the main ferromagnetic contribution along the *b*-axis corresponds to the BV of one IR (IR5), a second ferromagnetic contribution along the *c*-direction and the antiferromagnetic contribution leading to the presence of the (0 0 1) magnetic peak correspond to the two BVs of the second IR (IR3); Table 4 lists the used IRs and the results of the refinement.

Fig. 12a shows the fit of this model to the 2 K data, the resulting magnetic structure (Fig. 12b) is relatively simple, with

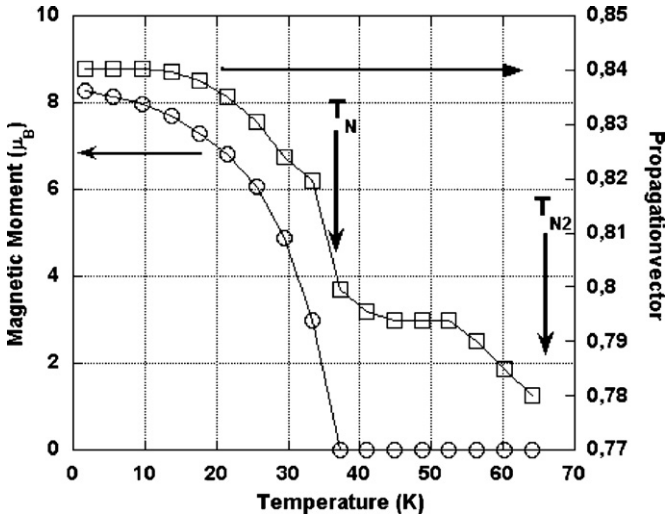

Fig. 10. Temperature dependence of the magnetic moment value and of the magnetic propagation vector of TbMgSn.

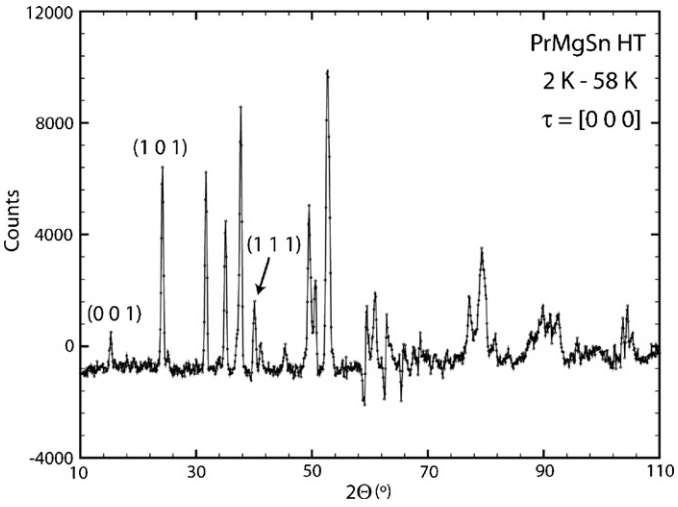

Fig. 11. Difference spectrum 2–58 K showing the purely magnetic scattering of PrMgSn (HT). The (0 0 1) reflection is forbidden in *Pnma* and indicates an antiferromagnetic contribution.

ferromagnetic components in the *b*- and *c*-directions and an antiferromagnetic coupling along the direction of the *a*-axis.

The total magnetic moment is with $\mu_{Pr} = 2.72(4)\,\mu_B$ close to the expected value of the Pr^{3+} ion. Refining the temperature dependent D1B data files individually, it was found that the antiferromagnetic component does not longer exist in the data set at $T = 16$ K. Furthermore the refinement revealed that the ferromagnetic component in *c*-direction has as well disappeared at this temperature. This indicates that PrMgSn-HT below $T = 52$ K adopts first a purely ferromagnetic structure (described by IR5), then at about $T = 15$ K a second magnetic coupling (corresponding to IR3) leads to the spin-canted magnetic structure. A signature of this magnetic transition has been seen as an anomaly in the magnetic data on PrMgSn-HT [8] where it had been still attributed to the presence of some impurity phase or to a small amount of the PrMgSn-LT phase.

3.2.5. CeMgSn

The thermodiffractogram of CeMgSn (not shown here) is not of sufficient statistics to clearly indicate the magnetic transition temperature. The difference spectrum created using the very long measurements at $T = 2$ K and 20 K (Fig. 13) shows a multitude of magnetic peaks at positions not corresponding to the nuclear Bragg peak positions, indicating thereby the antiferromagnetic nature of the magnetic coupling.

From the position of 12 magnetic peaks the magnetic propagation vector was determined to $\tau \approx [0\,0.19\,0.34]$. Two tiny peaks visible in the difference spectrum at about $2\theta = 13°$ and 14° had to be excluded, they are either belonging to a second magnetic propagation vector or to a magnetic impurity phase not detected in the high resolution data. We like to mention here that while the intensity of the strongest magnetic peak (at $2\theta \approx 38°$) amounts only to

Table 4
Basis-vectors (BV) of the two used irreducible representations (IR) for $\tau = [0\,0\,0]$ and for Wyckoff position *4c* of space group *Pnma* and results of the refinement of the coefficients of the BVs at $T = 2$ K.

	BV1	BV2	BV1
IR3		IR5	
x, y, z	1 0 0	0 0 1	0 1 0
$-x+1/2, -y, z+1/2$	−1 0 0	0 0 1	0 1 0
$-x, y+1/2, -z$	1 0 0	0 0 1	0 1 0
$x+1/2, -y+1/2, -z+1/2$	−1 0 0	0 0 1	0 1 0
$T = 2$ K	C (BV1)	C (BV2)	C (BV1)
(μ_B)	0.90(4)	0.90(8)	2.41(4)

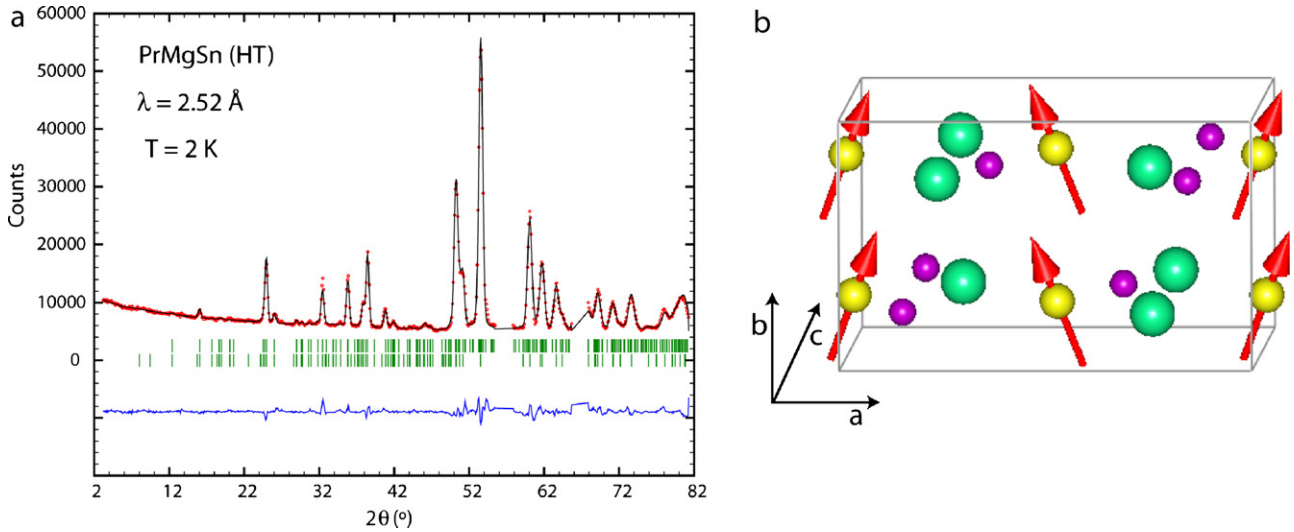

Fig. 12. (a) Observed (dots, red), calculated (line, black) and difference pattern of PrMgSn (HT) at 2 K. The tick marks indicate the calculated position of the nuclear Bragg peaks (upper row) and of the magnetic peaks (lower row). (b) Magnetic structure of PrMgSn (HT) at 2 K. (For interpretation of the references to colour in this figure legend, the reader is referred to the web version of the article.)

about 5% of the strongest nuclear Bragg peak it is more than ten times stronger than the two excluded tiny peaks. Magnetic symmetry analysis for the Wyckoff *4c* position in *Pnma* space group and $\tau = [0\ 0.19\ 0.34]$ shows that the atom site is split into two orbits and that there are two irreducible representations having each three basis-vectors (Table 5).

Testing the two possible models (IRs) against the recorded data the refinement converged smoothly using the three BVs of IR2. The refined spectrum of the 2 K data is shown in Fig. 14. As the nuclear scattering is largely dominating the spectrum, a second refinement was done using the difference spectrum (2–20 K). In this case one refines solely a magnetic phase and has to fix the scale factor to the value found in the refinement of the nuclear structure. This second refinement is shown as an insert in Fig. 14. The two orbits of atom sites were first forced to adopt the same coefficients for the three BVs in order to limit the number of free parameters for the magnetic phase refinement. This gave a reasonable fit with $R_{Mag} = 14\%$ and a maximum magnetic moment value of this amplitude-modulated structure of 2.24(2) μ_B, exactly the value expected for a Ce^{+3} ion (2.14 μ_B). The value of the magnetic propagation vector refined at 2 K to $\tau = [0, 0.1886(4), 0.3384(8)]$.

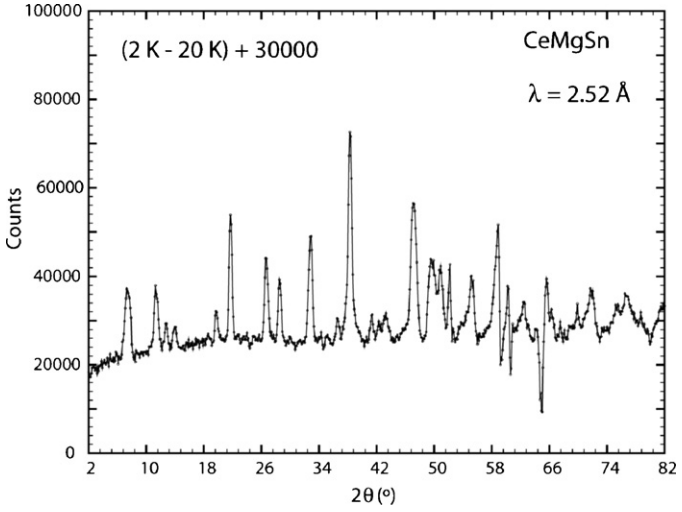

Fig. 13. Difference spectrum 2–20 K showing the purely magnetic scattering of CeMgSn.

A second refinement allowed the two orbits to have independent basis-vectors. This improved the refinement significantly ($R_{Mag} = 9\%$) but increased, however and as expected, the error bars of the determined coefficients and of the resulting total Ce magnetic moment. Table 5 includes the results of the two refinements; Fig. 15 displays the magnetic structure of the model with independent orbits. The magnetic structure is a sine wave type structure propagating in the *b*–*c* plane, with an additional antiferromagnetic coupling along the *a*-axis. A helix-type model can reasonably be excluded for the description of the magnetic structure of CeMgSn as the coefficients for the 3 basis-vectors are not equal precluding any equal moment solution.

3.3. Comparison of the magnetic structures

Rather small is the number of neutron diffraction studies on the magnetic structures of rare-earth equiatomic ternary RTX compounds, crystallizing with the CeScSi-type structure, that has been

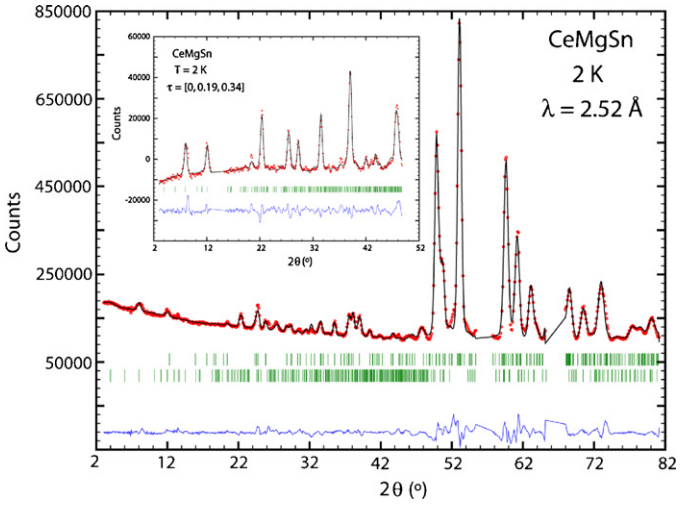

Fig. 14. Observed (dots, red), calculated (line, black) and difference pattern of CeMgSn at 2 K. The tick marks indicate the calculated position of the nuclear Bragg peaks (upper row) and of the magnetic peaks (lower row). The insert shows the refinement of just the magnetic phase using the difference spectrum (2–20 K). (For interpretation of the references to colour in this figure legend, the reader is referred to the web version of the article.)

Table 5
Basis-vectors (BV) of the two irreducible representations (IR) for $\tau = [0\,0.19\,0.34]$ and for Wyckoff position *4c* of space group *Pnma*, and results of the refinement of the coefficients (C) of the BVs using IR2 at $T = 2$ K. $\phi/2\pi$ is the phase between the two orbits of Ce atom site.

	BV1	BV2	BV3	
IR1				
x, y, z	1 0 0	0 1 0	0 0 1	
	0 0 0	0 0 0	0 0 0	
$-x+1/2, y+1/2, z+1/2$	−0.092 5 0 0	0 0.092 5 0	0 0 0.092 5	
	−0.995 7 0 0	0 0.995 7 0	0 0 0.995 7	
IR2				
x, y, z	1 0 0	0 1 0	0 0 1	
	0 0 0	0 0 0	0 0 0	
$-x+1/2, y+1/2, z+1/2$	0.092 5 0 0	0 −0.092 5 0	0 0 −0.092 5	
	0.995 7 0 0	0 −0.995 7 0	0 0 −0.995 7	
$T = 2$ K, IR2	C (BV1)	C (BV2)	C (BV3)	μ_{Ce}
1 orbit ($R_{Mag} = 14\%$) $\phi/2\pi = 0.04$	0.91(4)	1.28(2)	1.60(2)	2.24(2)
2 orbits ($R_{mag} = 9\%$) $\phi/2\pi = 0.05$				
Ce1 (0.020 1/4 0.678)	1.22(4)	0.78(8)	1.79(19)	2.30(20)
Ce2 (0.980 3/4 0.321)	0.35(6)	1.69(6)	1.43(18)	2.24(17)

so far reported in literature. In the series of the RZrSb compounds, the R = Tb and Dy ones adopt a purely ferromagnetic structure, with the moments aligned in the *c*-direction, HoZrSb is spin-canted with an additional antiferromagnetic coupling between the R-slabs while ErZrSb presents a helix-type structure within the *a*–*b* plane [13]. The total magnetic moments of the R^{3+} ions are significantly lower than the free ion values in these RZrSb compounds reflecting a rather strong influence of the crystal electric field (CEF). In the RScGe compounds series, the compounds with R = Tb and Nd are again purely ferromagnetic, with the moments in the *c*-direction (TbScGe) or inclined towards the *a*–*b* plane (NdScGe), while PrScGe seems to see an antiferromagnetic coupling leading to a doubling of the magnetic unit cell in the *c*-direction, with ferro- and antiferromagnetic couplings between adjacent R-slabs [14]. The magnetic structures found here for the RMgSn compounds are strongly differing in the sense that the dominating magnetic interaction (J3 in Fig. 1b) between the R-slabs is in all three compounds antiferromagnetic. As already mentioned before, the magnetic structure found for TbMgSn is not very different from the simple antiferromagnetic structure found for NdMgSn and PrMgSn (LT): main difference resides in the value of the magnetic propagation vector, $\tau = [0.84\,0\,0]$ for R = Tb, and $\tau = [1\,0\,0]$ for R = Pr (LT) and Nd, while the magnetic couplings in all three compounds are the same, with the ferromagnetic R-slabs being antiferromagnetically coupled in the *c*-direction (Figs. 5b and 9). The distance d_{J3} between the R-slabs varies between $5.87\,\text{Å} \leq d_{J3} \leq 5.66\,\text{Å}$ for the compounds of the RZrSb series (R = Tb, Nd and Pr), between $5.62\,\text{Å} \leq d_{J3} \leq 5.52\,\text{Å}$ for the compounds of the RScGe series (R = Pr, Nd and Tb) and between $5.42\,\text{Å} \leq d_{J3} \leq 5.33\,\text{Å}$ for the RMgSn compounds currently studied [R = Pr (LT), Nd and Tb]. This indicates that the reduced distance between neighbouring R-slabs might be responsible for the establishment of the antiferromagnetic coupling found in the RMgSn compounds.

Diffraction data on RPtSn [15,16], RNiSn [17,18] and RPdSn (R = Ce, Pr) [19,20] show that these equiatomic RTSn compounds with TiNiSi structure have unit cell parameters varying between $7.38\,\text{Å} < a < 7.54\,\text{Å}$, $4.52\,\text{Å} < b < 4.63\,\text{Å}$ and $7.60\,\text{Å} < c < 8.02\,\text{Å}$. Compared to the unit cell parameters listed in Table 1 one can see that while the unit cell *a*-parameter is only slightly enlarged in our RMgSn compounds (R = Ce, Pr (HT)) and the *b*-parameter is of similar size, the unit cell *c*-parameter has increased by about 15%. This makes it difficult to compare directly the magnetic structures of our two compounds with literature data. As a consequence of the enlarged unit cell *c*-parameter the R–R distances determining the J1 and J2 couplings (Fig. 1b and Table 1) become very similar in CeMgSn and PrMgSn (HT), while in the above mentioned other RTSn compounds these distances are different by about 20%. While CeNiSn which does not establish magnetic order down to lowest temperatures has stimulated a large interest as a so-called "Kondo insulator", CePdSn and CePtSn were found to be antiferromagnets adopting incommensurate magnetic structures with moments of about $1\,\mu_B$ [18,21,22]. The magnetic behaviour of CeMgSn is strongly differing as the magnetic moment value found at 2 K corresponds with $\mu_{Ce} = 2.2\,\mu_B$ to the Ce^{3+}

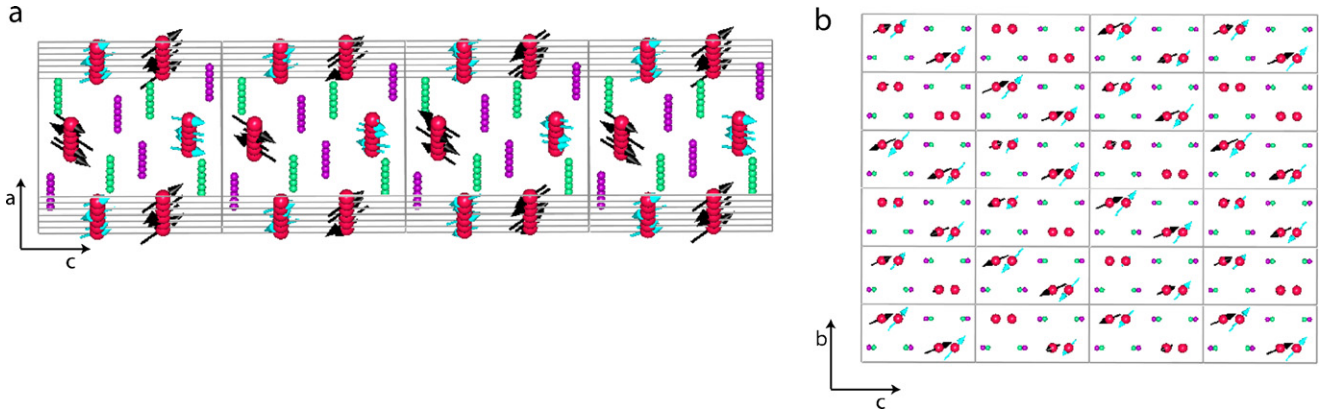

Fig. 15. Magnetic structure of CeMgSn. (a) Slightly inclined view onto the *a*–*c* plane showing the sine wave structure along the *b*-axis and the *c*-axis and the antiferromagnetic coupling in *a*-direction. Spins belonging to the same orbit have the same colour. (b) View onto the *b*–*c* plane showing the action of the magnetic propagation vector $\tau = [0, 0.19, 0.34]$.

free ion value and points to a strong localisation of the 4f electron.

Using the well known Bertaut notation of possible magnetic couplings for a fourfold site: G = S1–S2 + S3 – S4, C = S1 + S2 – S3 – S4, A = S1 – S2 – S3 + S4, F = S1 + S2 + S3 + S4 where S1–S4 are the Wykoff positions of the magnetic site, the magnetic structure found for PrMgSn (HT) can be classified as $C_xF_yF_z$. Looking at Figs. 1b and 12b one sees that J1 is positive while the antiferromagnetic coupling is introduced through J2. We have no knowledge of other PrTSn compounds with similar magnetic structure. PrPtSn [23] and PrNiSn [24] are not ordered magnetically at low temperature, while PrPdSn sees a commensurate collinear magnetic structure with $\tau = [0, ½, ½]$ and $\mu_{Pr} = 3.4\,\mu_B$ [20] pointing to the existence of magnetic couplings extending the nearest neighbour interactions.

4. Conclusions

The magnetic structure of the CeScSi-type RMgSn compounds with R = Tb, Nd and Pr sees the antiferromagnetic coupling of ferromagnetically coupled R-slabs. The magnetic propagation vector is $\tau = [1\,0\,0]$ for R = Nd, Pr and $\tau = [0.84\,0\,0]$ for R = Tb. The strongly enlarged distance between the R-slabs might be responsible for this antiferromagnetic coupling which is atypical for CsScSi-type compounds. TbMgSn, even above $T_N = 35$ K, shows strong antiferomagnetic correlations up to $T_{N2} \approx 65$ K. TiNiSi-type PrMgSn sees below $T_C = 52$ K a purely ferromagnetic structure which below $T = 15$ K changes to a structure with additional antiferromagnetic interactions. CeMgSn adopts a complicated sine wave antiferromagnetic structure with $\tau = [0, 0.1886(4), 0.3384(8)]$. In all five compounds the magnetic moment values are close to the free ion values of the R^{3+} ions pointing to the localised nature of the 4f electrons and to a small influence of the crystal electric field.

Acknowledgements

Work supported by the US DOE, Division of Materials Science and Engineering (Office of Basic Energy Science) under contract N° DE-AC02-07-CH11358.

The authors wish to thank the *Institut Laue Langevin*; Grenoble (France), the work being performed under the *Proposal N° 5-31-2064*.

References

[1] P. Manfrinetti, A. Provino, K.A. Gschneidner Jr., J. Alloys Compd. 482 (2009) 81–85.
[2] P. Lemoine, A. Vernière, J.F. Marêché, B. Malaman, J. Alloys Compd. 508 (2010) 9–13.
[3] A. Provino, K.A. Gschneidner Jr., P. Manfrinetti, J. Alloys Compd. 497 (2010) 131–138.
[4] P. Villars, L.D. Calvert, Pearson's Handbook of Crystallographic Data for Intermetallic Phases, 2nd ed., American Society for Metals, Metals Park, OH, 1991.
[5] CRYSTMET-The Metals Database, version 4.2.0, Toth Information System Inc., 2009.
[6] P. Villars, K. Cenzual, Pearson's Crystal Data (Crystal Structure Database for Inorganic Compounds), CD ROM software, version 1.2, 2008.
[7] A. Provino, S.K. Dhar, P. Manfrinetti, 37 Physical-Chemistry National Conference, February 24–29, 2008, Camogli (Genova), Italy.
[8] A. Provino, S.K. Dhar, P. Manfrinetti, K.A. Gschneidner Jr., submitted for publication.
[9] J. Rodriguez-Carvajal, Physica B 192 (1993) 55–69, http://www.ill.eu/sites/fullprof/php/downloads.html.
[10] L.C. Chapon, J. Rodriguez-Carvajal, FullProf Studio is a program of the FullProf Suite that is freely available in the site given in [9], unpublished.
[11] C. Ritter, Solid State Phenom. 170 (2011) 263.
[12] P. Schobinger-Papamantellos, K.H.J. Buschow, C. Ritter, J. Magn. Magn. Mater. 186 (1998) 21–32.
[13] A.V. Morozkin, K. Halich, R. Welter, B. Ouladdiaf, J. Alloys Compd. 393 (2005) 34–40.
[14] P. Manfrinetti, A.V. Morozkin, O. Isnard, P. Henry, A. Palenzona, J. Alloys Compd. 450 (2008) 86–91.
[15] D. Rafaja, V. Rejdák, B. Janoušová, P. Svoboda, V. Sechovský, J. Alloys Compd. 334 (2002) 50–52.
[16] B. Janoušová, P. Svoboda, V. Sechovský, K. Prokeš, T. Komatsubara, H. Nakotte, S. Chang, B. Ouladdiaf, I. Císařová, Appl. Phys. A 74 (2002) S731–S733.
[17] D. Rossi, R. Marazza, R. Ferro, J. Less-Common Met. 107 (1985) 99–104.
[18] A. Hiess, I. Zobkalo, M. Bonnet, J. Schweizer, E. Lelievre-Berna, F. Tasset, Y. Isikawa, G.H. Lander, J. Phys. Condens. Matter 9 (1997) 9321–9332.
[19] S.K. Malik, D.T. Adroja, S.K. Dhar, R. Vijayaraghavan, B.D. Padalia, Phys. Rev. B 40 (1989) 2414–2418.
[20] M. Kolenda, S. Baran, A. Oleś, N. Stüsser, A. Szytola, J. Alloys Compd. 269 (1998) 25–28.
[21] T.J. Hammond, G.A. Gehring, M.B. Suvasini, Phys. Rev. B 51 (1995) 2994–3002.
[22] H. Kadowaki, J. Phys. Soc. Jpn. 67 (1998) 3261–3266.
[23] Ch.D. Routsi, J.K. Yakinthos, E. Gamari-Seale, J. Magn. Magn. Mater. 110 (1992) 317–322.
[24] M. Kurisu, R. Hara, G. Nakamoto, Y. Andoh, S. Kawano, D. Schmitt, Physica B 312–313 (2002) 861–863.